Precise Measurement of Parity Nonconserving Optical Rotation in Atomic Thallium

N. H. Edwards,[1] S. J. Phipp,[1] P. E. G. Baird,[1] and S. Nakayama[2]
[1]*Clarendon Laboratory, Parks Road, Oxford OX1 3PU, United Kingdom*
[2]*Hyogo University of Teacher Education, 942-1 Shimokume, Yashiro-cho, Kato-gun, Hyogo 673-14, Japan*
(Received 5 October 1994)

We report a new measurement of parity nonconserving (PNC) optical rotation on the $6p_{1/2}$-$6p_{3/2}$ transition in atomic thallium near 1283 nm. The result expressed in terms of the quantity $\mathcal{R} = \mathrm{Im}\{E1^{\mathrm{PNC}}/M1\}$ is $-(15.68 \pm 0.45) \times 10^{-8}$, and is consistent with current calculations based on the standard model. In addition, limits have been set on the much smaller nuclear spin-dependent rotation amplitude at $\mathcal{R}_S = (0.04 \pm 0.20) \times 10^{-8}$; this is consistent with theoretical estimates which include a nuclear anapole contribution.

PACS numbers: 32.80.Ys, 11.30.Er

Theories of the electroweak interaction predict parity nonconserving (PNC) effects in atoms [1]. Recent measurements have been made in cesium [2] and thallium [3] using a Stark interference technique, and in bismuth [4,5], lead [6], and thallium [7] with optical rotation. Comparison of these results with calculations based on the neutral weak interaction provides an important low energy test of electroweak unification. We report here a new optical rotation measurement of the PNC optical rotation in the vicinity of the 1283 nm $M1$ transition in thallium, which is a factor of 5 more accurate than our earlier result [7]. The uncertainty is now at a level which is sensitive to radiative corrections and to a nuclear anapole contribution of the size predicted by atomic and nuclear theory [8].

The optical rotation arises because a small $E1^{\mathrm{PNC}}$ amplitude is mixed into the $M1$ transition which causes a difference in the refractive index of an atomic vapor for left- and right-handed circularly polarized light. Great sensitivity is required from the apparatus to detect the PNC signal since the peak amplitude of the rotation is only of order 10^{-7} rad per absorption length of vapor. The PNC signal may be written

$$\phi_P(\nu) = \phi_I(\nu) + \phi_S(\nu), \tag{1}$$

where $\phi_I(\nu)$ and $\phi_S(\nu)$ are the nuclear spin-independent and spin-dependent contributions, respectively. The nuclear spin-dependent part contains both the anapole and the electron-vector, nuclear-axial-vector terms. For a transition between states $|i\rangle$ and $|j\rangle$, these terms may be written in the following form:

$$\phi_I(\nu) = -p\mathcal{R} \sum_{F_i F_j} K_1(F_i, F_j) D_G(\nu_{ji} - \nu), \tag{2}$$

$$\phi_S(\nu) = -p\mathcal{R}_S \sum_{F_i F_j} K_S(F_i, F_j) D_G(\nu_{ji} - \nu). \tag{3}$$

In these expressions, the constant p is the number of absorption depths defined such that the fractional transmission α through the vapor is given by

$$\ln\alpha(\nu) = -p \sum_{F_i F_j} [K_1(F_i, F_j) + \chi^2 K_2(F_i, F_j)] L_G(\nu_{ji} - \nu). \tag{4}$$

Values of the angular factors, represented by the K_1, K_2, and K_S coefficients, for the transition of interest in thallium are given in Table I. The line-shape functions L_G and D_G are Doppler-broadened Lorentzian and dispersion curves, respectively; χ is the ratio of reduced $E2$ to $M1$ matrix elements.

Naturally occurring thallium has two isotopes, ^{205}Tl (70.5%) and ^{203}Tl (20.5%), both of which have nuclear spin $I = \frac{1}{2}$. For the transition of interest in thallium, the hyperfine (HF) structure consists of two well-resolved groups with a separation of approximately 21 GHz [9] (the ground state HF splitting), which we will refer to as the lower and upper (frequency) HF groups. The upper state HF splitting is much smaller (~500 MHz). Since the rotation profile within each of the HF groups has the same frequency dependence for spin-dependent and spin-independent terms, the two rotations cannot be distinguished by measurements on one HF group alone; the scan range of our laser is limited to one HF group. The values of $\mathcal{R}$ and $\mathcal{R}_S$ may be found by floating amplitudes $\mathcal{R}_L$ and $\mathcal{R}_U$ of the profile on the individual HF groups, and using the relationships

$$\mathcal{R} = \tfrac{3}{4}\mathcal{R}_L + \tfrac{1}{4}\mathcal{R}_U, \tag{5}$$

$$\mathcal{R}_S = \tfrac{1}{4}\mathcal{R}_L - \tfrac{1}{4}\mathcal{R}_U. \tag{6}$$

Experimental data were taken such that the final uncertainties of the rotation amplitude on lower and upper components were approximately in the ratio 1 : 3, which can be shown to be optimal for a determination of $\mathcal{R}$ by considering the statistical combination of errors of the terms in Eq. (5).

TABLE I. Angular coefficients for thallium transmission and PNC rotation profiles.

(F_i, F_j)	Character	K_1	K_2	K_S
(0, 1)	$M1$	0.1667	0.0000	−0.5000
(0, 2)	$E2$	0.0000	0.1000	0.0000
(1, 1)	$M1/E2$	0.0833	0.1500	0.0833
(1, 2)	$M1/E2$	0.4167	0.1500	0.4167

 0031-9007/95/74(14)/2654(4)$06.00

The apparatus and experimental procedure are based on the same principles as our earlier work [7]; the significant improvement in experimental accuracy compared to our previous result arises from many refinements to the apparatus. Principally these are the use of a new laser source and a much superior detector. The optical layout of the experiment is shown in Fig. 1. The laser source consists of a multiple-quantum-well InGaAsP semiconductor diode with an external cavity which produces 3 mW. In contrast to the distributed feedback (DFB) laser used in our previous work, frequency selective feedback from the cavity provides control of the output frequency and reduces the laser linewidth to much less than 1 MHz [10]. The low frequency jitter obtained with this arrangement results in a considerable improvement in signal-to-noise ratio compared to the DFB laser. The laser light passes through a single-mode, polarization-preserving fiber to reduce the effects of beam movements, before entering the polarimeter. The polarimeter consists of a pair of crossed polarizers between which are a Faraday modulator and an oven which contains thallium. The polarizer and analyzer each consist of a pair of 30°/60° calcite prisms. Following the design of Birich *et al.* [11], additional cuts were made in each prism to minimize interference effects caused by internal reflections.

The Faraday modulator consists of a rod of Hoya FR5 glass with end faces polished to create a trapezoidal shape, again to reduce interference effects. The modulator produces a sinusoidally varying rotation of peak amplitude $\theta_m = 6.1$ mrad, which was found to give an optimal signal-to-noise ratio. Details of the technique of using a Faraday modulator in optical polarimetry are given in [12].

As described in our earlier paper [7], a double oven arrangement allows the interchange of a tube containing thallium vapor with one containing a buffer gas (helium at a pressure of 30 Torr), without movement of any optical component. In this way, spurious optical rotations arising from interference effects in the polarizers and oven windows may be subtracted from the frequency dependent rotation signal. To obtain approximately 20 absorption depths on the lower HF component, an operating temperature of about 1200 K is required over the 450 mm of hot zone. A Mumetal shield is used to screen external magnetic fields, and a coil wound on the alumina tube containing thallium is used to apply small axial dc fields which may be used to cancel any residual magnetic field and to measure the Faraday effect.

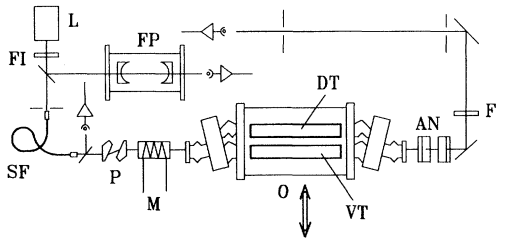

FIG. 1. Layout of the PNC experiment. Light from the laser L passes through an isolator FI before entering a single-mode optical fiber SF; a stabilized etalon FP is used to monitor the laser sweep. Between the crossed polarizers P and AN are a modulator M and a double oven arrangement O which contains a tube of thallium vapor VT and a dummy DT. The output from the polarimeter passes through an interference filter before reaching the main signal detector.

The beam transmitted through the oven passes through the analyzer and through an interference filter which reduces the amount of oven light and laser off-mode light incident on the detector.

The main signal detector consists of a fast InGaAs photodiode with an amplifier circuit containing a 500 MΩ feedback resistor; this detector-amplifier arrangement gives high gain with an excellent signal-to-noise ratio across a rotation spectrum despite the relatively low laser intensity. Two germanium photodiodes record the laser intensity and the transmitted intensity through a stabilized confocal etalon (FSR 375 MHz); the latter is used for calibration of the frequency scan.

The transmitted intensity $I(\nu, t)$ incident on the InGaAs photodiode may be written as

$$I(\nu, t) = I_0 \alpha(\nu) \{[\theta_m \sin\Omega t + \phi(\nu)]^2 + \xi^2\} + C, \quad (7)$$

where I_0 is the laser intensity, ξ^2 is the leakage through the crossed polarizers of the polarimeter ($\xi^2 \approx 10^{-7}$), and C results from background light. The angle ϕ has contributions from PNC ϕ_P, the Faraday effect ϕ_F, and background rotations ϕ_B which can arise from a variety of possible mechanisms, i.e.,

$$\phi(\nu) = \phi_P(\nu) + \phi_F(\nu) + \phi_B(\nu). \quad (8)$$

Experimental data are acquired by sweeping the laser across each hyperfine group of the transition and recording the signals from the detectors, normalizing for fluctuations in the laser intensity. The laser scans are calibrated by fitting a cubic polynomial to the centers of gravity of the etalon fringes. The spectra are then rebinned into equally spaced frequency channels. Vapor and dummy transmission signals are divided, and rotation signals subtracted. Doppler-broadened line profiles are then fitted to the transmission spectra to determine the Lorentzian and Gaussian linewidths, the frequency offset of the transition, and the number of absorption depths p. These parameters are then fixed and the rotation profiles fitted to obtain amplitudes of the parity rotation profile $\mathcal{R}$, longitudinal magnetic field B, and the background rotation, represented by a quadratic polynomial in frequency $\phi_B(\nu) = P_0 + P_1\nu + P_2\nu^2$. Typically $\phi_B(\nu)$ is no more than 0.1 μrad over the profile. As the signal-to-noise ratio is dependent on the transmission through the oven, and thus varies significantly over the profile, a weighted fit was used.

Examples of transmission and Faraday rotation profiles are given in Figs. 2 and 3. The Faraday rotation curve

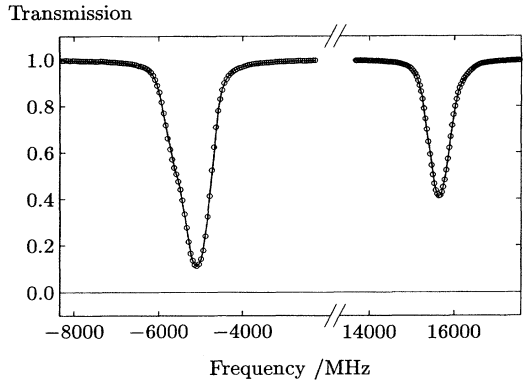

FIG. 2. Fitted experimental transmission spectrum at 4 absorption depths.

has a differential dispersion curve about a single frequency component and, being symmetric about line center, is thus largely orthogonal to the parity rotation, which is antisymmetric. We note that nonlinear Faraday effects including the effects of optical pumping observed in $E1$ transitions [13] are absent here; this is because the transition is relatively forbidden and the laser intensity very low. The goodness of fit (see Fig. 3) provides evidence for this.

A total of more than 2100 laser sweeps across the components of the thallium transition were superposed to form the spectrum shown in Fig. 4. The theoretical curve shown fits well to the experimental points, thus verifying our model of the data.

Thorough testing for the presence of possible systematic errors was carried out by analyzing the data in many different ways and looking for correlations, for example, with absorption depth and magnetic field. Among the systematic sources investigated were effects due to a transverse magnetic field (the Voigt effect), inhomogeneities in the vapor, nonuniformity of any magnetic field, and the presence of any off-mode laser light. We have successfully modeled and accounted for these phenomena. In particular, the optical rotation produced by a magnetic

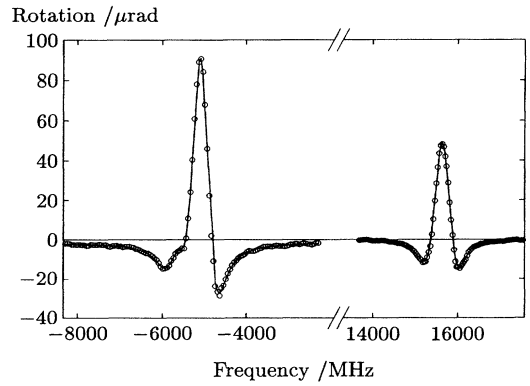

FIG. 3. Fitted experimental Faraday effect spectrum at 4 absorption depths with an axial magnetic field of 1.3 μT.

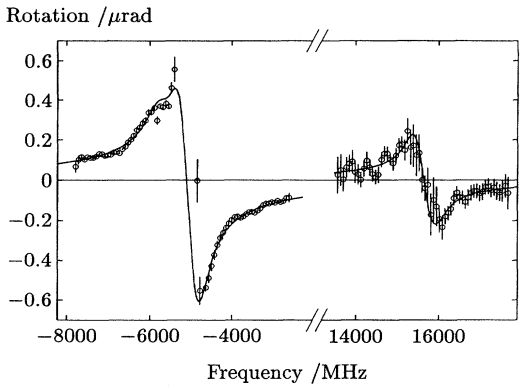

FIG. 4. A superposition of all the thallium PNC data on upper and lower hyperfine groups. A small residual Faraday effect ($B \sim 3$ nT) has been subtracted for clarity. The circles represent the experimental data and the error bars, the standard error in each frequency channel.

field at an arbitrary direction to the laser light propagation has been analyzed and will be the subject of a forthcoming paper.

During the acquisition of data, the optical components were regularly realigned to randomize as much as possible the vapor independent background rotation. In addition, rotation spectra taken under different polarizer and analyzer orientations were grouped to highlight certain systematic errors which include any Voigt effect. The data show (see Table II) that there is no evidence for such effects at the level quoted. The entire data set was fitted with modified weighting functions and different orders of polynomial background rotation ϕ_B to establish with confidence and reliability the estimates of uncertainty.

The overall calibration of the polarimeter was found by rotating the analyzer through a known angle using a precise rotation stage with a long lever arm. The mechanical calibration is consistent with an independent measurement obtained by fitting high field Faraday effect data to an accuracy of 1%. This additional uncertainty is included in our final results; our final values for the spin-independent and spin-dependent rotations are as follows:

$$\mathcal{R} = (-15.68 \pm 0.45) \times 10^{-8},$$

$$\mathcal{R}_S = (-0.04 \pm 0.20) \times 10^{-8},$$

where the errors quoted represent 1 standard deviation.

Table III shows the experimental results and theoretical calculations of $\mathcal{R}$ and $\mathcal{R}_S$ for the transition of interest. The

TABLE II. Variation of results with polarizer and analyzer orientations.

P	A	$\mathcal{R}_L/10^{-8}$	$\mathcal{R}_U/10^{-8}$
0°	90°	−15.2(6)	−15.0(2.1)
0°	270°	−16.3(7)	−14.1(0.9)
90°	0°	−15.5(4)	−16.4(1.2)
90°	180°	−16.4(7)	−17.7(1.3)

TABLE III. Recent experimental and theoretical values of $\mathcal{R}$ and $\mathcal{R}_S$ (in units of 10^{-8}).

Theory	$\mathcal{R}/10^{-8}$	$\mathcal{R}_S/10^{-8}$
[14] (1987)[a]	−15.1(0.4)	...
[19] (1990)[a]	−14.7(1.5)	...
[20] (1990)[a]	−17.7(1.6)	...
Mean[b]	−15.2(0.5)	...
[8] (1994)	...	−0.06(01)
Experiment	$\mathcal{R}/10^{-8}$	$\mathcal{R}_S/10^{-8}$
[7] (1991)[c]	−12.6(1.9)	...
This work	−15.68(0.45)	−0.04(20)

[a]This is calculated using a weak charge of $Q_W = -116.8$.
[b]This is a weighted mean of the above three theoretical results.
[c]This value is normalized to ^{205}Tl rather than a weighted mean of the two isotopes as quoted in [7].

most precise calculation to date is by Dzuba *et al.* [14] with an estimated uncertainty of 3%. Our new experimental results are consistent with the theoretical calculations to within the estimated uncertainties. Furthermore, we have now set a limit very close to that predicted for any nuclear anapole contribution [8].

The experimental and theoretical values of $\mathcal{R}$ can be used to estimate the mass of the Z boson [15], giving $M_Z = 89.9(1.9)$ GeV/c^2, using a value of $Q_W = -116.8$ from formulas in [16] which include radiative corrections (a contribution of around 6%). This low energy result is consistent with the current high energy value of 91.187(7) GeV/c^2. To date, the only published combination of low energy PNC experimental and theoretical results which is more precise than this is the Stark interference experiment on cesium [2], and the corresponding calculation by Blundell, Johnson, and Sapirstein [17]; in this case, the experimental accuracy of 2% is combined with a formidable atomic calculation which achieves a remarkable precision of 1%.

Our experimental result presents a challenge to atomic theorists to improve the precision of calculations of PNC in atomic thallium. With new developments in solid state lasers offering higher intensities, greater experimental accuracy in this element should certainly be feasible. Furthermore, thallium is a particularly interesting case in the context of the detection of a nuclear anapole moment [8,18].

PNC measurements [3] and calculations [14] have also been carried out on the forbidden $M1$ $6p_{1/2}$-$7p_{1/2}$ transition near 293 nm in thallium. A study of the PNC effects in the two transitions would provide a valuable consistency check of the two experimental techniques and the atomic calculations.

We are indebted to K. Cameron of BT Research Laboratories for his help and participation in this work and his close collaboration with one of us (N. H. E.) through a CASE studentship scheme. We also acknowledge support from SERC in the form of a research grant, a Senior Visiting Fellowship (S. N.), and two research studentships (N. H. E. and S. J. P.). Finally, we are grateful to Professor P. G. H. Sandars for his continuing interest in this work.

[1] M. A. Bouchiat and C. C. Bouchiat, Phys. Lett. **48B**, 111 (1974).
[2] M. C. Noecker, B. P. Masterson, and C. E. Wieman, Phys. Rev. Lett. **61**, 310 (1988).
[3] P. S. Drell and E. D. Commins, J. Phys. B **53**, 968 (1984).
[4] M. J. D. Macpherson *et al.*, Phys. Rev. Lett. **67**, 2784 (1991).
[5] R. B. Warrington, C. D. Thomson, and D. N. Stacey, Europhys. Lett. **24**, 641 (1993).
[6] D. M. Meekhof *et al.*, Phys. Rev. Lett. **71**, 3442 (1993).
[7] T. D. Wolfenden, P. E. G. Baird, and P. G. H. Sandars, Europhys. Lett. **15**, 731 (1991).
[8] I. B. Khriplovich, Report No. BINP 94-56 (unpublished).
[9] M. Grexa, G. Hermann, and G. Lasnitschka, Phys. Rev. A **38**, 1263 (1988).
[10] R. Wyatt, Electron. Lett. **21**, 658 (1985).
[11] G. N. Birich *et al.*, Sov. Phys. JETP **60**, 442 (1984).
[12] T. D. Wolfenden, P. E. G. Baird, J. A. Deeny, and M. Irie, Meas. Sci. Technol. **1**, 1060 (1990).
[13] I. O. G. Davies, P. E. G. Baird, and J. L. Nicol, J. Phys. B **202**, 5371 (1987).
[14] V. A. Dzuba, V. V. Flambaum, P. G. Silvestrov, and O. P. Sushkov, J. Phys. B **20**, 3297 (1987).
[15] P. G. H. Sandars, J. Phys. B **23**, L655 (1990).
[16] B. W. Lynn and P. G. H. Sandars, J. Phys. B **27**, 1469 (1994).
[17] S. A. Blundell, W. R. Johnson, and J. Sapirstein, Phys. Rev. Lett. **65**, 1411 (1990).
[18] C. Bouchiat and C. A. Piketty, Phys. Lett. B **269**, 195 (1994).
[19] A. C. Hartley, E. Lindroth, and A.-M. Mårtensson-Pendrill, J. Phys. B **23**, 3417 (1990).
[20] A. C. Hartley and P. G. H. Sandars, J. Phys. B **23**, 4197 (1990).